machines

MDPI

Article

Closed-Loop Transient Longitudinal Trajectory Tracking for Connected Vehicles

Lingyun Hua and Guoming Zhu *

Department of Mechanical Engineering, Michigan State University, East Lansing, MI 48824, USA; hualingy@msu.edu
* Correspondence: zhug@msu.edu

Abstract: Vehicle longitudinal trajectory tracking plays a significant role in developing eco-routing and autonomous driving systems to handle various disturbances and uncertainties (e.g., road grade, gust wind, etc.) that are often ignored by the optimization strategies used to generate reference controls and trajectories. In this paper, based on a linearized vehicle model with the help of feedback linearization, a linear quadratic integral tracking (LQIT) control is utilized to generate regulation laws to minimize the tracking error of optimal speed or brake distance trajectories, respectively, and maintain brake safety. A unified Kalman filter is used to estimate system states based on noisy measurements. Both acceleration and deceleration LQIT controls are designed to handle the change of upper-level optimal control strategies to varying traffic. Simulation and co-simulation studies validated the proposed LQIT control strategies in Simulink with the SUMO traffic model using a real-world map under manipulated driving conditions. The simulation results show that under changing traffic conditions, the LQIT acceleration control is able to reduce the static tracking error by 99.8%, compared with the vehicle controlled only by the high-level optimal acceleration control without a trajectory tracker, achieving less tracking error and overshoot than using a PI control. The LQIT deceleration control reduces the brake distance error by 48% over the optimal deceleration control alone and ensures a safer brake distance than a coupled PI control. The traffic model used in the SUMO co-simulation confirms the capability of handling varying traffic for the developed LQIT control strategies.

Keywords: connected and autonomous vehicles; linear quadratic integral tracking; feedback linearization; speed tracking control; distance tracking control

check for updates

Received: 15 January 2025
Revised: 13 February 2025
Accepted: 17 February 2025
Published: 19 February 2025

Citation: Hua, L.; Zhu, G. Closed-Loop Transient Longitudinal Trajectory Tracking for Connected Vehicles. *Machines* **2025**, *13*, 163. https://doi.org/10.3390/machines13020163

Copyright: © 2025 by the authors. Licensee MDPI, Basel, Switzerland. This article is an open access article distributed under the terms and conditions of the Creative Commons Attribution (CC BY) license (https://creativecommons.org/licenses/by/4.0/).

1. Introduction

Concerns about global warming and pollution emissions have lead to the increased utilization of electric vehicles (EVs) to significantly reduce transportation greenhouse emissions. Note that EVs, equipped with vehicle connectivity and autonomous driving systems, are capable of significantly reducing energy consumption for a given travel plan [1,2]. Extensive research has been dedicated to reducing energy consumption by developing high-level controls that provide reference trajectories, such as eco-route planning providing eco-route and reference speed [2], low-level path motion control [3], and vehicle speed/distance reference generation [4] based on the real-time traffic information obtained from the vehicle sensors and connected system. In addition to energy consumption, the vehicle driving stability is also critical; thus, path and speed planning methods have also been investigated in [5]. However, trajectory planning is usually at a high enough level that can be influenced by disturbances and uncertainties. Therefore, a well-designed trajectory tracking control is necessary.

With the provided speed/distance references, one of the longstanding focuses regarding vehicle control is accurately tracking the given reference signal under disturbances such as gust wind, road grade, etc. To track speed reference, traditional PID control has been adopted to minimize the tracking error between the target and current speed [6] to increase tracking accuracy. Model-based control, such as linear quadratic regulation (LQR) control, is a popular method capable of maintaining good tracking accuracy with a smooth tracking process [7], but it cannot eliminate tracking error due to the lack of integral control. In order to improve tracking accuracy, a detailed vehicle model, including engine and transmission [8], is adopted, along with robust LQR [9]. The above control methods are developed by the ideal driving environment assumption. However, under real-world driving conditions, the road conditions (e.g., road grade, tire-road friction, gust wind, etc.) change constantly, and as a result, the unmodeled nonlinearity could undermine the performance of the developed control strategy. To handle the unmodeled nonlinearity and provide sufficient control torque, model predictive control (MPC) is usually adopted along with a comprehensive powertrain and vehicle dynamic model [10]. In addition, MPC is capable of including constraints and handling uncertainties to improve vehicle stability and performances [11,12]. However, without integral tracking control, the tracking accuracy cannot be ensured due to potential model mismatches such as vehicle mass variation and/or gusting wind. QPSOMPC-based feedback control with a bicycle vehicle model and steering system model can perform stable and accurate trajectory tracking, even during turning [13]. Whereas the high nonlinearity in the model and high order system result in a high computational load which could make the method a challenge for strict real-time implementations such as speed tracking at higher speed.

Another method for vehicle speed tracking is to utilize future information (see [14]), based on the information from connected communications, to regulate the vehicle to reference speed under transient operation, assuming the existence of mild noise. However, the availability of future information could make this method a challenge. Model-based reinforcement learning was also applied to track speed reference by using a trained feedback gain well-tuned for a specific vehicle [15]. The challenge of using learning methods is balancing the depth of exploration and the extended duration required for the learning process. In summary, the developed speed tracking control methods are relatively accurate due to the implementation of comprehensive vehicle models, dealing with system noise and uncertainties, and utilizing future road traffic information. However, a complex model could result in a high model order, making it hard to design implementable control strategies adapting to real-time driving conditions. In addition, these control algorithms, mentioned above, only track the vehicle speed. However, due to the rapidly shifting traffic, driving safety will require tracking vehicle distance since tracking vehicle speed cannot avoid collision or stop at the desired position (e.g., stopping at a traffic light). Therefore, precise tracking of both vehicle speed and distance references in real time and the ability to handle emergencies (e.g., vehicle cut-in) are very important.

This paper proposes a linear quadratic integral tracking (LQIT) control to directly track an optimal reference speed or distance trajectory for driving in longitudinal (or with small turning angle) for route and speed optimization [16], which is not targeted to improve driving stability [17]. Note that under distance tracking, speed tracking is inherited. The speed or distance reference signal used in this paper is from the speed or distance trajectory provided by the high-level optimal vehicle motion controller designed for vehicle acceleration and braking; see our early work [18]. Given the desired speed and driving distance from the connected vehicle system and its own sensor signals, the optimal acceleration control generates the optimal speed trajectory; the optimal brake control optimizes both speed and distance trajectories to minimize the energy consumption [18].

Note that both strategies are updated in real time to maintain driving safety under traffic conditions. Both optimal controls provide the associated optimal torque according to the speed or distance trajectory. Since the optimal controls are generated based on a simple analytic model, due to modeling errors and the existence of system noises and uncertainties (such as gust wind, road grade, etc.), the optimal control torque may not track the desired speed or distance reference, and a regulation/tracking control law is needed to track the speed or distance reference to ensure driving safety under disturbances and changing traffic conditions. As a result, the LQIT control is designed to overcome the model mismatch, uncertainties, and system noises by minimizing a quadratic cost function of the integrated tracking and torque errors to improve system tracking accuracy. In addition, the braking control is constrained by a preview system that keeps tracked distance not exceeding the reference so that the vehicle will not stop beyond the stop line at the traffic light. The proposed LQIT control strategy is developed based on a simple longitudinal vehicle dynamic model and is evaluated in MATLAB and SUMO (Simulation of Urban MObility) co-simulations by comparing the performance of the proposed LQTI tracking control and the optimal control [18] without a trajectory tracker.

The main contributions of this paper are described as follows: (a) developing a LQIT speed tracking control to minimize reference speed tracking error with feedback linearization that handles the vehicle system's nonlinearity; (b) further reducing the tracking errors caused by model mismatches, system noise, and driving environmental uncertainties such as wind and road grade; (c) developing the LQIT acceleration and deceleration controls using the same state estimator, model, and control framework, allowing simple implementation and enabling seamless switching by simply adjusting parameter values; (d) utilizing tracking distance constraints for the transient LQIT deceleration control to make sure that the vehicle stops before the desired stop-line; and (e) evaluating tracking performance by co-simulation studies in MATLAB/Simulink and Simulation of Urban MObility (SUMO) under disturbed and emergency driving situations.

This paper is organized as follows. Section 2 presents the simple vehicle longitudinal dynamic model, and Section 3 reviews the optimal controls in [18] that provide reference speed and distance trajectories. Section 4 proposes the LQIT tracking controls for both acceleration and braking (deceleration), respectively. The simulation investigation results in Matlab/Simulink are presented in Sections 5 and 6 gives the co-simulation results with real-world map information. Finally, Section 7 provides some conclusive discussions.

2. Vehicle Dynamics Model

Assuming that the electric motor (or motors) is the power source of the target electric vehicle used to generate the propulsion torque for the acceleration and regenerative torque during braking, the vehicle dynamics are described below.

$$m\dot{v} = \frac{Tr_d}{r} - F_r - F_a - F_g \tag{1}$$

$$\begin{aligned} F_r &= mgc_r cos\theta \\ F_g &= mgsin\theta \\ F_a &= 0.5c_d\rho a_f v^2 \end{aligned} \tag{2}$$

$$c_r = a + bv^2 \tag{3}$$

where m and v are the vehicle mass and speed; T is the total driving torque applied to the powertrain or total regenerative (braking torque); r_d is the driveline gear ratio from the powertrain to wheels; r is the wheel radius; F_r and F_g are the rolling resistance force and the force along the track caused by the vehicle's weight on the road, respectively; c_r is the

rolling resistance coefficient approximated by a second-order polynomial with parameters $a = 0.0136, b = 0.31 \times 10^{-8}$ (see [19]); g and θ are the gravity acceleration and road grade angle, respectively; and the air drag force F_a is modeled with air density ρ, the air drag coefficient c_d, and vehicle front area a_f. Note that the calculation of aerodynamic drag does not take wind speed into account due to the fact that most production vehicles typically lack wind speed sensors, with the assumption that this information is also not available from the connected system.

3. Optimal Control Review

As mentioned in the introduction, the proposed LQIT control strategy tracks vehicle speed or the distance reference generated by two optimal control strategies. The architecture of the proposed cooperative control is shown in Figure 1. As shown in the top-dashed block, the "optimal controls" block [18] generates the optimal control reference with a given target vehicle speed v_{tar} or distance d_{tar} provided by the high-level connected planning system; two LQIT controllers are developed to track either target (acceleration speed or deceleration distance) in an infinite time horizon.

The "optimal controls" block consists of a nonlinear quadratic tracking (NQT) acceleration control and braking (deceleration) control based on minimal principle (MP). Both optimal controllers are designed based on a simple vehicle dynamic model shown in Equation (1). The NQT acceleration control tracks the v_{tar} and the MP brake control stops the vehicle at target distance d_{tar}. Analytic solutions are solved in open loop for both optimal controllers in [18] and can be implemented and updated for real-time applications with a sampling time of 0.1 s since these solutions are analytic. As a result, both optimal control laws can be adapted to changing references from the high-level planning system based on the shifting traffic information. The detailed control strategies can be found in [18].

The outputs of the two open-loop optimal controllers are the speed reference v_{ref} (for acceleration and deceleration), target stop distance d_{ref} (deceleration), and associated with the torque T_{ref} references for the entire control periods. Note that the output torque reference is constrained by the powertrain limitation [18]. However, the calculated optimal torque reference may not be accurate due to the existence of modeling error and unknown disturbances w, leading to tracking error. Even though the optimal controls are able to update the control laws in real time and can eventually reach the targets, the accumulated control error may delay the time taken for the vehicle to reach its target, result in extended brake distance that could lead to undesirable collision during vehicle following, or stop beyond the stop-line at traffic lights. Therefore, in the lower diagram with solid lines in Figure 1, the proposed LQIT controls with feedback linearization adjusts the torque reference to minimize the accumulated error between actual vehicle speed v_{real} (or distance d_{real}) and speed reference v_{ref} (or target distance d_{ref}). In this case, the vehicle can remain on the target trajectory provided by the "optimal controls".

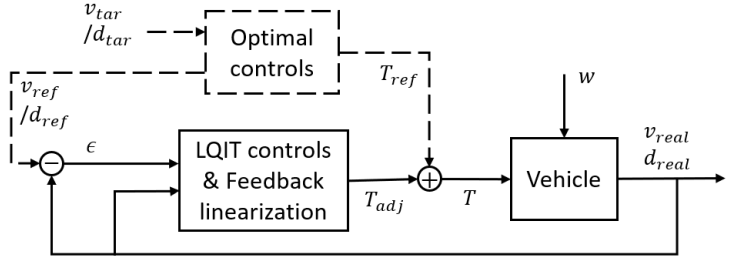


Figure 1. System architecture of trajectory tracking control.

4. Trajectory Tracking Control

In this section, the methodologies of the proposed LQIT trajectory tracking controls are introduced. The control strategy is separated into the following two parts: LQIT acceleration and braking controls due to different system models used for speed tracking during acceleration and target distance control under braking (deceleration). The system models are built based on the simple vehicle dynamics model introduced by Equation (1) in Section 2.

4.1. Linear Plant Model for LQIT Design

Since the system model in Equation (1) is nonlinear, there are a few approaches to linearizing this model for the linear control design. However, direct linearization through Taylor expansion will result in a linear model with a varying parameter (vehicle speed) called the LPV model, which cannot be used for the LQTI control developed for linear time-invariant systems. In this paper, a feedback linearization approach is used after Taylor expansion. Note that the constant terms F_r, F_g, and F_a are compensated in the optimal control laws as drive and brake torques and are denoted by T_{ref} in this study [18]. Let states $\delta x_1 = d - d_{ref}$ and $\delta x_2 = v - v_{ref} = \delta v$ represent the vehicle distance and speed errors, respectively. In this study, we use d to represent the driving distance and v for vehicle speed. As a result, model (1) can be linearized for the given speed trajectory v_{ref} as follows. Here we use δu to represent the torque and serve as the control law.

$$m\delta\dot{v} = \frac{r_d}{r}\delta u - (2mgb\cos\theta + c_d\rho a_f)v_{ref}\delta v \tag{4}$$

where $\delta u = T - T_{ref} - rF_g/r_d$. Note that the optimal control [18] generating T_{ref} assumes that $F_g = 0$. That is, it is not compensated in the optimal control T_{ref}, and hence, is compensated with feedback linearization. Our future work will focus on including $F_g = mg\sin(\theta)$ and wind speed to generate T_{ref}. The above model can be reorganized into the following state-space model.

$$\delta\dot{x}_p = \begin{bmatrix} 0 & 1 \\ 0 & 0 \end{bmatrix}\delta x_p + \begin{bmatrix} 0 \\ \frac{r_d}{rm} \end{bmatrix}\delta u - \begin{bmatrix} 0 \\ \frac{c_d\rho a_f}{m} + 2gb\cos\theta \end{bmatrix} v_{ref}\delta v \tag{5}$$

where $\delta x_p = [\delta x_1, \delta x_2]^T$. The above state space model can be reorganized into the following form.

$$\delta\dot{x}_p = \begin{bmatrix} 0 & 1 \\ 0 & 0 \end{bmatrix}\delta x_p + \begin{bmatrix} 0 \\ \frac{r_d}{rm} \end{bmatrix}\delta u_f + \begin{bmatrix} 0 \\ d \end{bmatrix}\delta w \tag{6}$$

$$\delta u_f = \delta u - \delta u_c,\ \delta u_c = \frac{r}{r_d}(2mg + c_d\rho a_f)v_{ref}\delta v \tag{7}$$

where $\delta w = v_{ref}\delta v$, and $d = 2g(1 - cos\theta)$. The above model can be discretized as follows with sample period $t_s = 0.05$ s, with notation δ dropped.

$$x_p(k+1) = A_p x_p(k) + B_p u_f(k) + D_p w(k) \tag{8}$$

where

$$A_p = \begin{bmatrix} 1 & t_s \\ 0 & 1 \end{bmatrix}, B_p = \begin{bmatrix} 0 \\ \frac{t_s r_d}{rm} \end{bmatrix}, D_p = \begin{bmatrix} 0 \\ t_s d \end{bmatrix}$$

and x_p is the discretized state of δx_p, u_f for δu_f, and w for δw.

4.2. LQIT Acceleration Control

Note that the optimal control only provides the reference speed since the distance under acceleration is not critical. Thus, the tracking error for acceleration process $\epsilon_a(k) = v_{ref}(k) - x_2(k)$ measures the difference between reference speed v_{ref} and vehicle speed x_2. To eliminate the static tracking error, the accumulated tracking error $\epsilon_{a,a}(k)$ is defined below.

$$\epsilon_{a,a}(k+1) = \sum_{i=0}^{k} t_s \epsilon_a(i) = \epsilon_{a,a}(k) + t_s \epsilon_a(k) \tag{9}$$

Then, a new discrete state $\epsilon_{a,a}$ can be added to the plant model to form the discrete-time LQIT acceleration control design model below, based on model (8).

$$\begin{aligned} x_a(k+1) &= \begin{bmatrix} 1 & t_s & 0 \\ 0 & 1 & 0 \\ 0 & -t_s & 1 \end{bmatrix} x_a(k) + \begin{bmatrix} 0 \\ \frac{t_s f_d}{rm} \\ 0 \end{bmatrix} u_{fa}(k) + \begin{bmatrix} 0 \\ t_s d \\ 0 \end{bmatrix} w(k) \\ &= A_a x_a(k) + B_a u_{fa}(k) + D w(k) \end{aligned} \tag{10}$$

where $x_a(k) = [x_p^T(k), \epsilon_{a,a}(k)]^T$ is the state vector and the actual control signal $T_{adj} = \delta u(k) = u_{fa}(k) + \delta u_c(k)$ (see Figure 2), where u_{fa} represents u_f for acceleration control; $\delta u_c(k)$ is due to feedback linearization and is calculated for each time step using the measured vehicle speed. To avoid exceeding the vehicle capability, saturations are added to the applied and regenerative torque, which are the maximum drive torque for the acceleration control and maximum brake torque for the deceleration control. The speed trajectory tracking problem under acceleration is formulated to minimize the following quadratic cost function.

$$J_a = \sum_{k=0}^{\infty} x_a^T(k) Q_a x_a(k) + u_{fa}^T(k) R_a u_{fa}(k) \tag{11}$$

where the weighting matrix Q_a is symmetric and semi-positive definite. Note that only the weighting for accumulated state error $\epsilon_{a,a}$ is nonzero to avoid over-definition, and R_a is a positive number. For this problem, the selected weightings are listed below.

$$Q_a = 5 \times 10^3 \times \begin{bmatrix} 0 & 0 & 0 \\ 0 & 0 & 0 \\ 0 & 0 & 1 \end{bmatrix}, \quad R_a = 1 \tag{12}$$

With the augmented system (10), the LQIT control law can be solved using the typical LQR solution directly (see [20]), where the optimal control is

$$\begin{aligned} u_{fa}^*(k) &= -K_a \begin{bmatrix} \hat{x}_p(k) \\ \epsilon_{a,a}(k) \end{bmatrix} \\ &= -(R_a + B_a^T P_a B_a)^{-1} B_a^T P_a A_a \begin{bmatrix} \hat{x}_p(k) \\ \epsilon_{a,a}(k) \end{bmatrix} \end{aligned} \tag{13}$$

where $\hat{x}_p(k)$ is the estimated plant state vector by a Kalman estimator (to be designed in the next subsection), gain matrix K_a is a 1×3 row vector, and the positive semi-definite matrix P_a satisfies the following Riccati equation. Note that $\epsilon_{a,a}(k)$ is the accumulated tracking error calculated by (9) and does not need to be estimated.

$$P_a = A_a^T P_a A_a - A_a^T P_a B_a (R_a + B_a^T P_a B_a)^{-1} B_a^T P_a A_a + Q_a \tag{14}$$

As mentioned before, only the speed reference is used for the acceleration control; thus, the distance state x_1 is not needed, and the output distance is not measured for the acceleration control. Due to the selection of Q_a, the weighting for the vehicle distance state x_1 is zero, and as a result, this state is not observable, the designed control gain is in the format $K_a = [0, *, *]$, where "$*$" represents the nonzero element. Therefore, the distance state x_1 is not involved in the acceleration control.

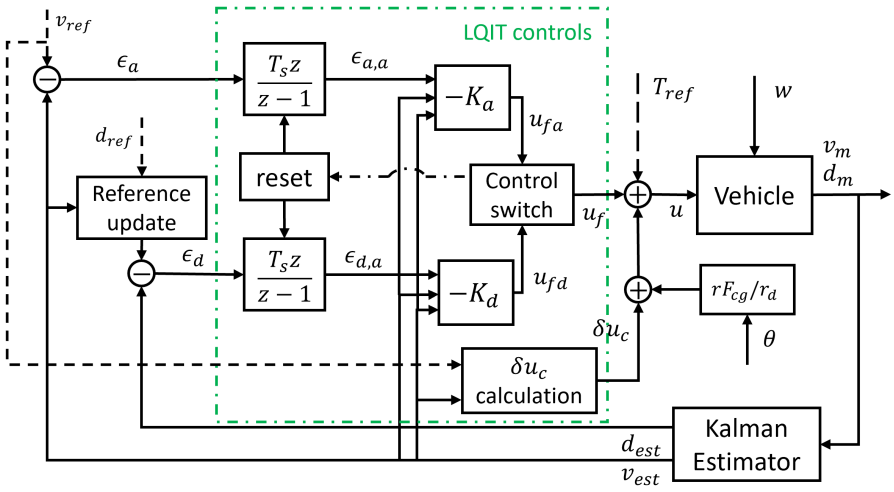


Figure 2. Closed-loop control system architecture.

4.3. LQIT Deceleration Control

For the LQIT deceleration control, both the speed and distance references are provided by the optimal control. Considering the speed and distance are correlated and the deceleration distance is more critical for safety, the tracking error for the deceleration process is defined by $\epsilon_d(k) = d_{ref}(k) - x_1(k)$, which measures the difference between the reference distance d_{ref} and vehicle distance x_1. To eliminate the static tracking error, the accumulated tracking error $\epsilon_{d,a}(k)$ is defined below.

$$\epsilon_{d,a}(k+1) = \sum_{i=0}^{k} t_s \epsilon_d(i) = \epsilon_{d,a}(k) + t_s \epsilon_d(k) \tag{15}$$

Then, a new state $\epsilon_{d,a}$ can be added to the plant model to form the LQIT deceleration control design model below.

$$x_d(k+1) = \begin{bmatrix} 1 & t_s & 0 \\ 0 & 1 & 0 \\ -t_s & 0 & 1 \end{bmatrix} x_d(k) + \begin{bmatrix} 0 \\ \frac{t_s f_d}{rm} \\ 0 \end{bmatrix} u_{fd}(k) + Dw(k) \tag{16}$$

where $x_d(k) = [x_p^T(k), \epsilon_{d,a}(k)]^T$ is the state vector, u_{fd} is u_f for the deceleration control and $D = [0, t_s d, 0]^T$ is the same as the definition given in Equation (10).

Then, with the same feedback compensation as the acceleration control, the distance trajectory tracking problem for deceleration can be formulated as

$$J_d = \sum_{k=0}^{\infty} x_d^T(k) Q_d x_d(k) + u_{fd}^T(k) R_d u_{fd}(k) \tag{17}$$

with constraint $\epsilon_d(k) \geq 0$, where Q_d is symmetric semi-positive definite matrix and R_d is a positive number. Both weightings are chosen as below.

$$Q_d = 1 \times 10^3 \times \begin{bmatrix} 0 & 0 & 0 \\ 0 & 0 & 0 \\ 0 & 0 & 1 \end{bmatrix}, \quad R_d = 1 \times 10^{-3} \tag{18}$$

Note that in the deceleration control, distance state x_1 is one of the system outputs and is observable even though the corresponding weighting is zero in Q_d, the resulting control gain K_d is a 1×3 row vector with all nonzero elements. Note that the optimal LQIT deceleration control gain K_d can be designed in the same way as the optimal LQIT acceleration controller. The resulting control is

$$u_{fd}^*(k) = -K_d \begin{bmatrix} \hat{x}_p(k) \\ \epsilon_{d,a}(k) \end{bmatrix} \tag{19}$$

4.4. Kalman Estimator Design

Before we can apply the designed control laws, the plant state x_p needs to be estimated, considering the vehicle system and measurement noises. For this paper, it is assumed that the vehicle speed can be measured and the driving distance is the integration of speed. Note that the speed measurement v_m can be obtained by integrating the accelerometer signal, directly based on the wheel speed, or based on the Global Navigation Satellite System (GNSS). However, the accelerometer could have bias, integrating the signal may cause signal drifting, and high-accuracy GNSS is usually unavailable on production vehicles. The sensor fusion method can not only improve measurement accuracy but also reduce measurement noise [21]. In this case, the Kalman state estimator based on the system model with a noisy wheel speed measurement is utilized to provide the state estimate $\hat{x}_p$ of x_p. Note that $x_p = \delta x_p = [\delta x_1, \delta x_2]^T$ and that state δx_2 is calculated by subtracting the measured speed from the reference speed v_{ref}.

Note that the estimation of plant state x_p is valid for both acceleration and deceleration problems. As a result, a single estimator for estimated state $\hat{x}_p$ is used for both acceleration and braking feedback controls. The Kalman state estimator is designed based on the discrete-time plant model (8) and is modified as follows, with the added measurement equation below.

$$\begin{aligned} x_p(k+1) &= A_p x_p(k) + B_p u_f(k) + D_p w_p(k) \\ z(k) &= C_p x_p(k) + n(k) \end{aligned} \tag{20}$$

where $w_p(k)$ and $n(k)$ are the system and measurement noises with their intensity matrices W_p and N, respectively; $C_p = [0,\ 1]$. With the above discrete-time system with system and measurement noises, the Kalman state estimator can be designed based on reference [22] that is highlighted below.

$$\begin{aligned} \hat{x}_p(k|k-1) &= A_p \hat{x}_p(k-1|k-1) + B_p u_f(k) \\ P(k|k-1) &= A_p P(k-1|k-1) A_p^T + W_p \\ K(k) &= P(k|k-1) C_p^T S^{-1}(k) \\ S(k) &= C_p P(k|k-1) C_p^T + N \\ P(k|k) &= (I - K(k) C_p) P(k|k-1) \\ \hat{x}_p(k|k) &= (I - K(k) C_p) \hat{x}_p(k|k-1) + K(k) z(k) \end{aligned} \tag{21}$$

where $\hat{x}_p(k|k-1)$ and $\hat{x}_p(k|k)$ are the predicted and updated state estimates, respectively; $P(k|k-1)$ and $P(k|k)$ are the predicted and updated estimate covariances; and K is the optimal Kalman gain.

Therefore, based on the methodologies developed above, a control system architecture diagram is summarized in Figure 2, where the inputs are the references v_{ref}, d_{ref}, and T_{ref}. By comparing the v_{ref} (or d_{ref}) to the estimated speed v_{est} or (d_{est}) from the Kalman estimator, the transient tracking errors ϵ_a (or ϵ_d) can be obtained. After obtaining the accumulated tracking error through the discrete-time integration process, the LQIT control u_f can be calculated by multiplying the estimated state $\hat{x_p}$ and $\epsilon_{a,a}$ (or $\epsilon_{d,a}$) to the control gain K_a (or K_d); see Equations (13) and (19). Note that the acceleration and deceleration controls are switched according to the command from high-level controllers and the switch in control resets the discrete-time integrator. Note that T_{adj} in Figure 1 is the summation of u_f, δu_c calculated by (7) using v_{est}, and rF_{cg}/r_d; see also Figure 2. Adding T_{adj} and T_{ref}, the total powertrain torque that powers the vehicle can be obtained.

4.5. Reference Modification for Deceleration LQIT Control

As mentioned in the problem formulation for deceleration tracking control in Section 4.3, the transient tracking error constraint $\epsilon_d \geq 0$ needs to be satisfied. However, due to the nature of linear quadratic control, the error could oscillate around the target trajectory, and it is not guaranteed that $\epsilon_d \geq 0$, which is not desirable since it could lead to an accident or stop over the stop line at traffic light. This can be demonstrated by the deceleration example presented in Figure 3, where the vehicle is required to brake from an initial speed of 15 m/s and stop within 50 m.

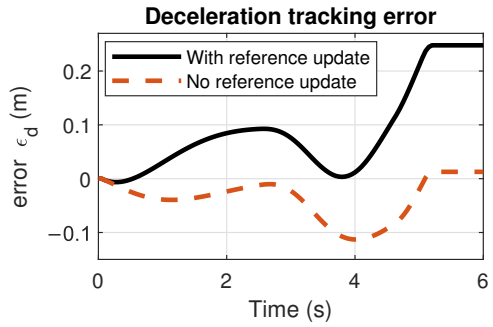


Figure 3. Deceleration tracking error comparison.

Without reference modification, the red-dashed curve (transient tracking error ϵ_d) in Figure 3 is negative until the 5th second, which breaches the constraint and may cause a collision during vehicle following. As observed, the amplitude of error increases after the 3rd second due to the application of smaller brake torque than that required by the control logic in the optimal deceleration control (see [18]) due to unknown disturbance, leading to increased negative tracking error. In addition, this situation continues until the end of the control period, when both vehicle speed and distance are approaching their targets, and with a low vehicle speed and a short distance to the target, the brake torque does not have enough freedom to be adjusted to track the target distance. To resolve this issue and avoid stopping distance overshooting by the LQIT control, a reference modification method is proposed; see block 'Reference update' in Figure 2.

Considering the error oscillates around its target $\epsilon_d = 0$ since the LQIT control is able to maintain the error within a certain range, the optimal distance reference can be reduced by a small δ value so that the entire oscillation of tracking error ϵ_d stays below the target. That is, the distance reference is modified as shown in the equation below.

$$d^*_{ref} = \max(d_{ref} - \delta, 0), \delta \geq 0 \tag{22}$$

In addition, since the distance reference at the beginning of the braking process is still far from the stop line, the constraint ($\epsilon_d \geq 0$) need not be met, but it will be strictly met when the vehicle approaches its target distance (stop line). Meanwhile, a sudden drop in distance reference could result in a large torque adjustment from the LQIT control, leading to discomfort. To avoid this, the δ value needs to be increased gradually. Thus, a function of δ is developed based on multiple simulation studies; see Equation (23) below.

$$\delta = \min(c_1 c_2 / v_{est}, c_2) \tag{23}$$

where coefficient $c_1 = 5$ and the maximum value of δ is chosen to be $c_2 = 0.2$, so that the brake distance to the stop line is expected to be close to +0.2 m to the target distance d_{ref} (or stop line) with acceptable driving safety. Note that these two coefficients can be calibrated experimentally. The proposed reference update method is studied through simulations, and the resulting tracking error, the solid curve, is shown in Figure 3, where the error ϵ_d is compared to the original distance reference. It can be seen that the vehicle stops at 5.2 s and the final tracking error is $\epsilon_d = 0.24$ m ≥ 0 due to the updated distance reference. As a result, the tracking error over this driving process remains positive, attributed to the reference modification/update method.

5. Simulation Results

In order to evaluate the performance of the proposed control strategy, simulations are carried out in MATLAB/Simulink R2020a first. The simulation step is set to be $\Delta t = t_s = 0.05$ s. The main vehicle parameters used are given in Table 1.

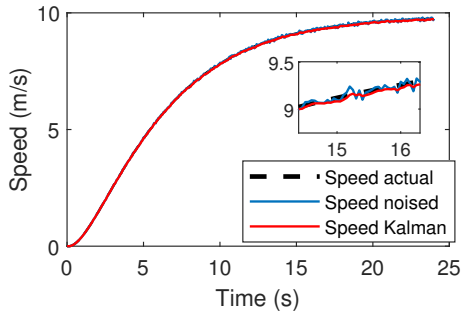
Table 1. Key simulation parameters.

Vehicle Parameter	Value	Vehicle Parameter	Value
Vehicle mass m	1600 kg	Wheel radius r	0.38 m
Total drive torque	525 Nm	Vehicle front area a_f	3.12 m^2
Total brake torque on powertrain	2734 Nm	Air drag coefficient c_d	0.37
Driveline gear ratio r_d	3.27		

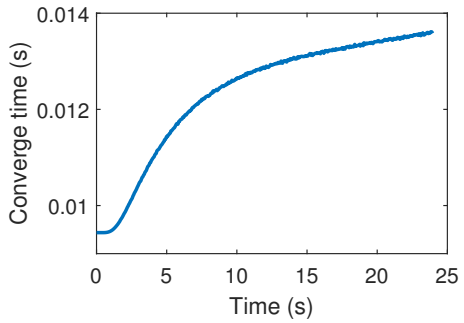
To validate the designed LQIT controls, the two optimal controls for acceleration and deceleration introduced in Section 3 and [18] are adopted as the baseline controls. For the purpose of comparison, two PI controllers for acceleration and deceleration are used to track the speed and torque references from the optimal controls. The powertrain output torque to wheels, generated by the optimal LQIT and PI controls, are applied to the vehicle plant model (1). The resulting vehicle speed, torque, and driving distance are compared for using optimal control strategy in Section 3, the one combing the optimal and LQIT controls in Sections 3 and 4, and the one combing the optimal and PI controls. To simulate modeling errors in real-world vehicle applications with varying vehicle parameters, the rolling resistance coefficients $a = 0.012$ and $b = 0$, defined in (3), are used in the optimal controls. Note that for the actual vehicle plant model $a = 0.0136$ and $b = 0.31 \times 10^{-8}$ based on [19]. In addition, the 1% error of vehicle mass is added to the vehicle plant to simulate the mass changes such as fuel usage. Note that the longitudinal wind speed v_w is used to calculate the air drag force F_a during the evaluation simulation, the new equation for air drag force F_a^* is provided by Equation (24) below. To simulate the measurement noise on vehicle speed, a Gaussian noise with zero mean and standard deviation of 1% of the speed. This setup is applied to all the simulations in this paper.

$$F_a^* = 0.5 c_d \rho a_f (v + v_w)^2 \tag{24}$$

Before the performance comparisons, the Kalman estimator is evaluated. The test vehicle is accelerated from 0 to 10 m/s. The speed results are shown in Figure 4a, where the estimated speed (Kalman speed) reduces the noise from the noised speed and is closer to the actual speed. The mean estimation error is 0.02 m/s with a variance of 3.05×10^{-4}. The max error is 0.07 m/s, which is within the estimation error tolerance of 0.1 m/s. Figure 4b shows the converge time of the estimator, which is faster than the sampling time in order to maintain high accuracy in measurement and respond very fast to the speed changes. The converge rate decreases with the increase in vehicle speed since the variance of the measurement noise changes along with the vehicle speed but is still very fast, as expected.



(**a**)



(**b**)

Figure 4. (**a**) Vehicle speeds estimation. (**b**) Converge time of the designed Kalman estimator.

Then, the simulations for both the acceleration and deceleration controls are conducted for a typical driving scenario, where the vehicle is driving, following a straight trajectory on a road with a road grade $\theta = 0$ and a gusting wind moving in alignment with the vehicle direction ($v_w \leq 0$). The wind speed with a peak value $max(|v_w|) = 10$ m/s is time-varying, as shown in Figure 5, and is used for both the acceleration and deceleration simulations.

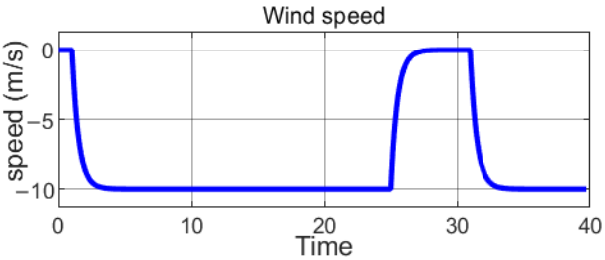
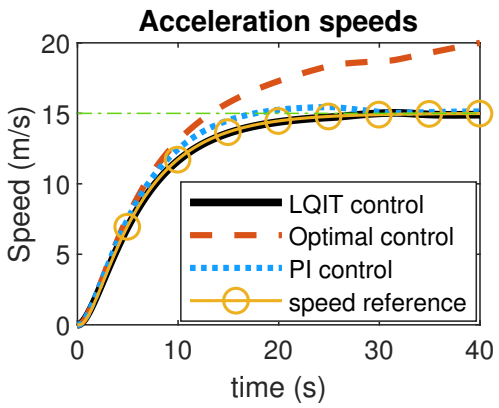


Figure 5. Gust wind speed profile.

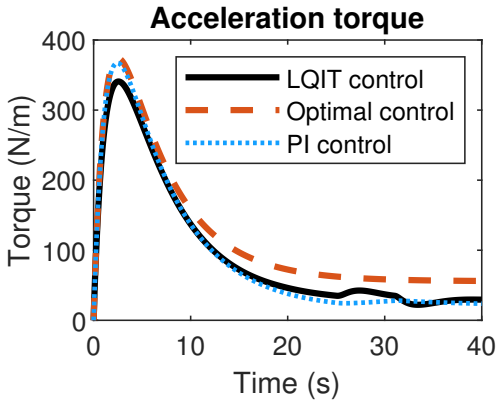
5.1. LQIT Acceleration Control

In this simulation, the target speed for the controlled vehicle is 15 m/s and the initial vehicle speed is 0 m/s, with the gust wind profile defined in Figure 5. The optimal acceleration control [18] provides both the reference speed and torque. The resulting vehicle

speed signals for the optimal (only), LQIT, and PI controls are presented in Figure 6a and the associated control torques (optimal, LQIT, and PI) are shown in Figure 6b.



(**a**)



(**b**)

Figure 6. (**a**) Vehicle speeds of the acceleration test with gusting wind. (**b**) Total driving torque applied in this test.

In Figure 6a, the green dash-dotted line denotes the target final speed of 15 m/s and the yellow line with circles is the reference speed from the optimal control [18]. It can be seen that the speed of the LQIT control matches the reference one well and converges to the final speed of 15.01 m/s after 35 s. Meanwhile, the speed of optimal control (without LQIT) exceeds the target speed after the 13th second and keeps increasing to 19.15 m/s at the 35th second due to the added gust wind. The PI control is designed to compensate for the speed error, as well as the LQIT control, and it is capable of regulating the vehicle speed to the target speed. However, an overshoot appears due to the integration action in the PI controller, which may cause safety issues and increase the energy consumption. Figure 6b describes how the controls respond to the added gust wind. By comparing it with the torque of the optimal control (red-dashed curve), it can be seen that the PI controller uses a similar torque to that of the optimal control, but the LQIT control reduces the driving torque between the 2nd and 4th second, because the wind speed changes rapidly from 0 m/s to -10 m/s during this period. The tailwind results in less air drag, leading to reduced driving torque to achieve the target acceleration. Then, the drive torque of LQIT control gradually converges to about 35 Nm to maintain the target vehicle speed and then increases to 50 Nm between the 25th and 31st second due to the changing gust wind in this period. The PI controller also reduces the torque more than the LQIT control since the 10th second, but it still leads to speed overshoot. Contrarily, the optimal control without LQIT does not change according to the changing gust wind speed. As a result, the LQIT

control achieves a mean tracking error of 0.036 m with a variance of 0.005, both of which are smaller than those from the PI control, which has a mean tracking error of 0.491 m and a variance of 0.077. The simulation results show that the LQIT acceleration control reduces the static tracking error by 99.8% over the optimal control without LQIT, demonstrating a better tracking performance than the PI control. The results indicate that the proposed LQIT acceleration control can minimize the tracking error of the reference speed and handle disturbances such as varying gust wind.

5.2. LQIT Deceleration Control

With the same driving scenario set up as that for acceleration, the vehicle is required to decelerate from an initial speed of 15 m/s until it fully stops (0 m/s) at the stop line with a target braking distance of 50 m. The optimal braking control [18] provides the distance reference for both the LQIT and PI deceleration controllers to track. Here, a couple of PI controllers are used since there are two references, speed and distance, to track. The outer loop of the PI controller tracks the distance and the inner one tracks the speed. The resulting vehicle speeds and brake distances of the optimal (only), LQIT, and PI controls are compared in Figure 7a and the associated brake control torques are presented in Figure 7b.

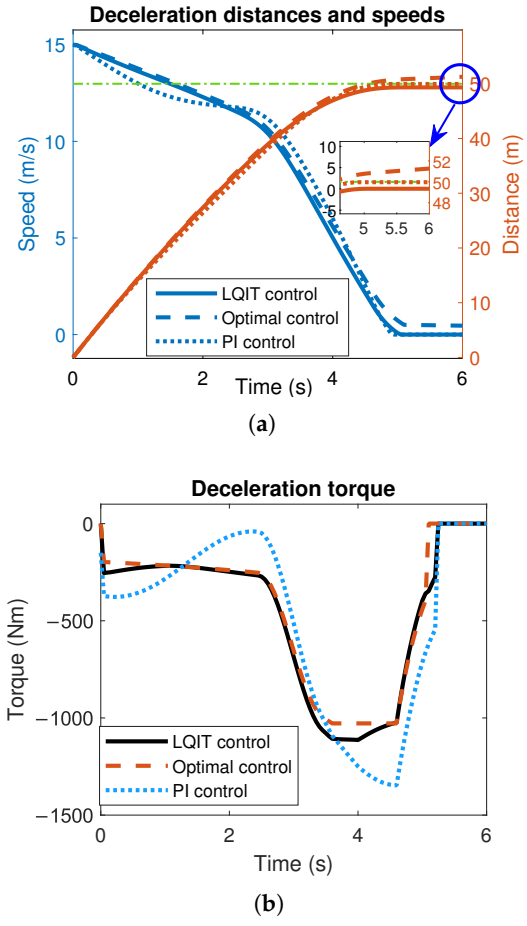


Figure 7. (**a**) Brake distances and speeds of the deceleration test with gusting wind. (**b**) Total brake torque applied in this test.

In Figure 7, the solid curves are speed, distance, and torque signals from the LQIT deceleration control. The dashed curves denote the results from optimal control without a trajectory tracker, the dotted lines are from the PI control, and the dash-dotted line is the target of the brake distance (stop line). The entire deceleration process takes 5.2 s and the gust wind speed for this braking process is the signal in Figure 5 between zero and

5.2 s. It can be seen from the speed responses in Figure 7a that, in the first 3 s, the vehicle speed with LQIT control is slightly slower than that of the optimal control, and it can be inferred from the torque plot in Figure 7b that the applied torques from both control strategies are almost the same at the first 3 s and the LQIT control uses more brake torque at the beginning due to the δ distance compensation (see Equation (23)). After the 3rd second, when the gust wind speed reaches its peak, the LQIT control utilizes more brake torque than that from the optimal control between the 3rd and 4.6th second, resulting in a faster reduction of speed than that of optimal control. Then, the brake torques of both controllers are reduced as both speed and distance are approaching their targets. At the end of the simulation, the optimal control stops the vehicle at a distance of 51.3 m and the stop distance error of 1.3 m is because the optimal control does not consider the gust wind; however, the LQIT control is able to stop the vehicle at a distance of 49.4 m before the stop line (see the zoomed plot of Figure 7a, which satisfies the requirement of not exceeding the target distance (stopping before the stop line). On the other hand, at the beginning, the PI control mainly follows the distance reference and slows down faster than the other controls, as shown in Figure 7a. At around the 2nd second, the brake distance of the PI control is below the reference distance; thus, it reduces the brake torque until the 3.5th second (See Figure 7b), resulting in the brake distance being slightly longer than that in the LQIT control. Eventually, the PI control is capable of stopping the vehicle right at the target distance. However, since the coupled PI controls operate sequentially to prioritize distance tracking, it cannot adequately follow the reference optimal trajectories and loses optimality compared to the LQIT control. As a result, the LQIT deceleration control, which tracks both speed and distance references simultaneously, achieves better tracking performance than the PI control. Meanwhile, the LQIT deceleration control improves the final tracking distance accuracy by 48% over the optimal control and stops before the stop line without overshooting. This simulation validates that the designed LQIT deceleration control is capable of slowing down the vehicle as needed under disturbances such as gust wind.

6. Co-Simulation Results

In the previous section, the proposed LQIT control works well under a manipulated driving scenario for acceleration and deceleration. To further validate the LQIT control's ability to handle real-world driving conditions, the traffic simulator, Simulation of Urban MObility (SUMO) [23], is used for performance validation.

SUMO is a platform that simulates the traffic environment and vehicle dynamics over a real-world map. The traffic environment data (information on roads and obstacles) and vehicle states (speed and position) are available to be retrieved and updated through SUMO by simulating the data communication in the connected vehicle system. In addition, the server of SUMO, Traffic Control Interface (TraCI), makes it possible to deliver traffic data from SUMO to MATLAB/Simulink and send back the control inquiries to change the motion of the ego vehicle in SUMO, which makes it convenient to design and evaluate the developed control strategy in MATLAB/Simulink in a real-world driving environment. Therefore, in this paper, SUMO is adopted to create a real-world driving scenario for evaluating the designed control strategies with a co-simulation platform of MATLAB/Simulink and SUMO.

6.1. Simulation with Road Grade

In this co-simulation study, the selected map in the SUMO simulation environment is located within an area of Ann Arbor, MI (USA); see Figure 8a. The elevation of this area is shown in the red box in Figure 8b. The elevation data are obtained from Shuttle Radar Topography Mission (SRTM) [24]. The testing road is defined by the origin–destination

pair, marked by "A" and "B" in Figure 8a. The test road has a length of 164 m and its road grade between points A and B is shown in Figure 9 with a peak grade of 12.5% and a minimum grade of 2.2%. Under this driving scenario, zero wind speed and obstacle-free (no traffic) conditions are assumed. Both acceleration and deceleration using the proposed LQIT control are co-simulated in this investigation, and they are compared with the PI controls.

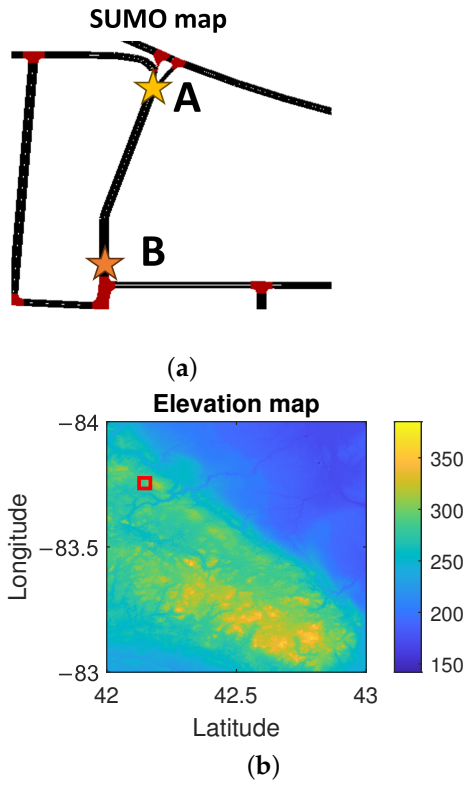


Figure 8. (**a**) The real-world map used in SUMO. (**b**) Elevation map from SRTM.

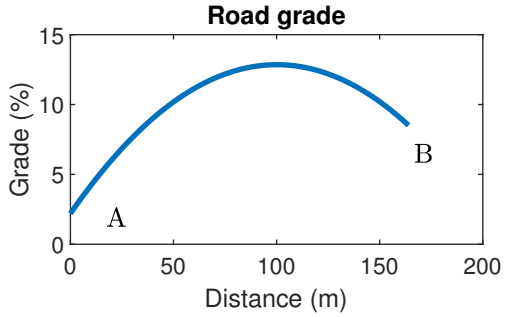


Figure 9. Approximated real-world elevation for test road.

In the simulation study of an acceleration process, the vehicle is required to drive from point A to B with an increasing elevation as shown in Figure 9. Note that the length of this road is 164 m. The initial vehicle speed is 0 m/s and the target speed is 10 m/s. The simulation results are shown in Figure 10a,b.

In Figure 10a, the speed of the LQIT control tracks the speed reference well (yellow circled curve) and reaches the target speed. Furthermore, its distance to the green dotted line at the 24th second indicates a tracking error of 0.06 m/s. However, the optimal controlled speed accelerates quickly and reaches 11.5 m/s at the end of the road in 21 s. As a result, the final speed when using the optimal control exceeds the target speed by 1.5 m/s. The PI control exceeds the target speed as well. Thus, the LQIT acceleration control reduces the tracking error by 96% over the optimal control and 4.4% over the PI control. From

the plot of the powertrain output torque signals of both controls in Figure 10b, it can be seen that the optimal control without LQIT applies more torque than the LQIT control during the entire acceleration period, which is due to two main factors. One is that the HJB solution from the optimal control in [18] assumes the steady-state solution, but as the road grade rapidly changes, this assumption is no longer true, leading to optimal control error; the other is due to the model mismatch in gravity resistance and rolling resistance. The PI control follows the torque reference for the first 5 s due to the proportional gain; then, the integration gain helps reduce the torque to be closer to the LQIT control while still exceeding the target, whereas the LQIT control adjusts the control torque even when the optimal control is not accurate at the beginning. Finally, the LQIT control achieves a mean tracking error of 0.017 m with a variance of 0.002, both of which are smaller than those of the PI control, which has a mean tracking error of 0.524 m and a variance of 0.027.

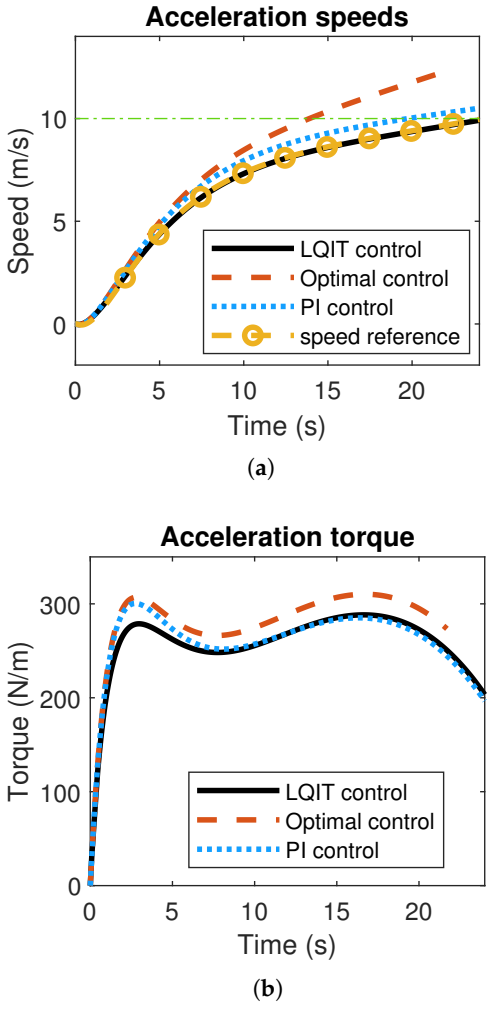
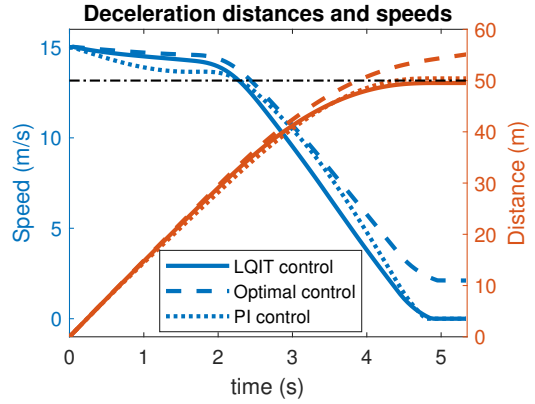


Figure 10. (**a**) Vehicle speed in the acceleration test with road grade. (**b**) Total driving torque applied in this test.

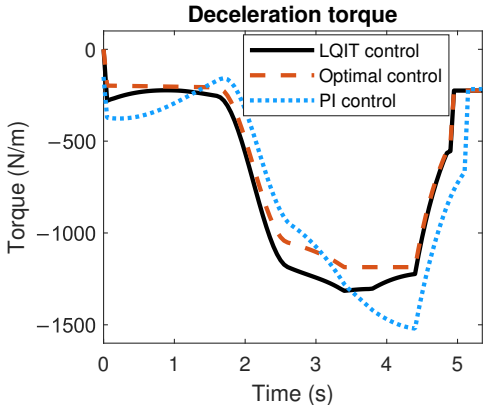
The co-simulation of the deceleration control is conducted on the same road as the acceleration, where the vehicle is driven downhill from point B to A so that the road grade becomes negative. The vehicle speed is reduced from 15 m/s down to 0 m/s. The target deceleration distance is set to be 50 m. The speed and distance trajectories of the LQIT, optimal, and PI controls are shown in Figure 11a; Figure 11b compares the corresponding braking torques applied during the deceleration process.

From Figure 11a, it can be seen that both the LQIT and PI controls are able to slow down the vehicle to its target speed at the 4.95th second. The total brake distance of the

LQIT control is 49.5 m, with a final tracking error of 0.5 m, and the PI control stops the vehicle at 50.4 m, slightly exceeding the target brake distance. However, the optimal control without LQIT can only reduce the vehicle speed down to 2.1 m/s and ends up with a braking distance of 54.5 m, which is over the target brake distance. This is not acceptable since it could cause an accident. From Figure 11b, it can be observed that the applied torque from the LQIT deceleration control is more than that of the optimal control in the first 4.5 s, since the high gravity force caused by the steep road grade requires more brake torque to slow down the vehicle. The applied torque of the PI control is lower than the other controls due to the proportional gain in the first 1.5 s. Then, the applied PI torque is higher than the other two controls until the 3rd second due to distance tracking error, and the PI control uses less torque than at least one of the other two controls, which enables the control to stop the vehicle and approach the target distance. The operations of the PI controls can undermine the optimality from the optimal reference trajectories and cause potential safety issues. According to these results, it can be concluded that the LQIT deceleration control can handle the varying road grade by reducing the static distance tracking error by 88.9% over the optimal control and ensuring driving safety during the deceleration process.



(**a**)



(**b**)

Figure 11. (**a**) Brake distances and speeds of the deceleration test with road grade. (**b**) Total brake torque applied in this test.

6.2. Simulation with an Obstacle

For the purpose of validating the capability of handling changing traffic scenarios, the proposed acceleration control is tested in a simulation environment with an obstacle on the road due to vehicle cut-in. The controlled vehicle needs to accelerate from rest to the target speed of 15 m/s on a straight road. In this scenario, at the 7th second, a vehicle in front cuts in but within a safe distance to the controlled vehicle so that no emergency brake is

needed. This change reduces the target speed to 12 m/s. After the 9th second, the front vehicle leaves the lane, and the target speed is changed back to 15 m/s. Since the optimal acceleration control is able to handle similar situations, as verified in [18], and the LQIT acceleration control tracks the speed reference from the optimal control, the performance of the LQIT control is evaluated based on the reaction time and tracking error. The simulation results are shown in Figure 12.

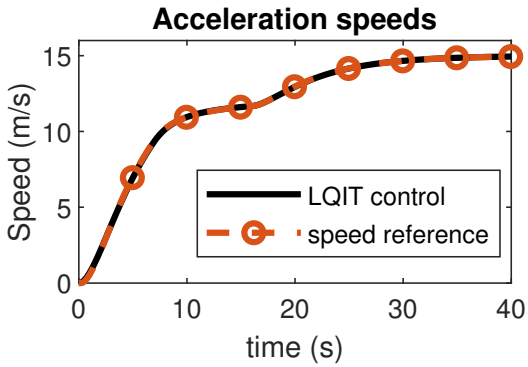


Figure 12. Acceleration control for vehicle cut-in.

Figure 12 compares the controlled vehicle speed with that of the target speed reference. It can be seen that the acceleration rate is reduced at once when the speed reference is changed after the 7th second, at which the front vehicle cuts in. Then, the controlled vehicle maintains a mild acceleration rate until the 16th second when the vehicle starts to track the original target speed. The co-simulation result shows that the vehicle speed tracks the reference speed well without any lag (or high tracking error), indicating that the proposed LQIT acceleration control is able to properly track the vehicle speed when traffic shifts.

Another simulation with shifting traffic is conducted for the LQIT deceleration control. This simulation assumes that there are no gust wind and road grade (zero). The controlled vehicle was required to decelerate from 15 m/s down to 0 m/s within a braking distance of 50 m. In this driving scenario, a vehicle will suddenly cut in at the 2.5th second after the deceleration process starts. Then, the vehicle brakes to maintain a safe distance from the one in front (cut-in) of it until both vehicles fully stop. As a result, after the vehicle cuts in, the target brake distance is reduced by 3.5 m to maintain the safe interval between two vehicles, factoring in the length of the front vehicle. The optimal deceleration control has the capability to handle a sudden vehicle cut-in in real time, which was demonstrated in [18]. In this simulation, the optimal control provides the speed and distance references before and after the vehicle cuts in for the LQIT deceleration control to track. The simulation results are shown in Figure 13.

In Figure 13, the dashed curves are the reference signals and the solid ones denote the results from the LQIT control. It can be seen from the plot that the controlled vehicle is slowing down with small errors to the references caused by the control overshoot. At the 2.5th second, the front vehicle cuts in and the optimal control reacts immediately by performing an emergency brake that reduces the speed from 11.6 m/s to 8.8 m/s between the 2.5th and 2.7th second. It can be seen that the speed from the LQIT control drops quickly along with optimal control, with a small tracking error to the reference. After the 2.7th second, the controlled vehicle follows the distance reference generated by the optimal control until both vehicles stop. The target distance reference at the end of the simulation is 46.4 m and the LQIT control stops at 45.8 m. In the entire process, the brake distance of the LQIT control is lower than the reference, with a final stop distance error of 0.7 m to ensure a safe stop. This simulation indicates that the proposed LQIT deceleration control has the ability to handle sudden reference changes due to vehicle cut-in.

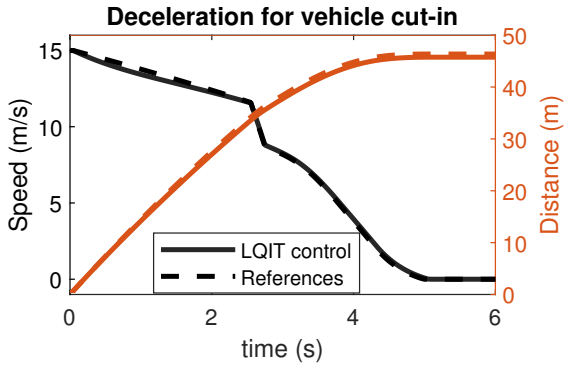


Figure 13. Deceleration control for vehicle cut-in.

7. Conclusions

This paper proposed a linear quadratic integral tracking (LQIT) control during both acceleration and deceleration to reduce the tracking error to the reference signal and to minimize the final tracking error of the target vehicle. Meanwhile, the LQIT control can provide robust tracking performance under model mismatches and environmental uncertainties such as varying vehicle mass due to fuel usage and variations of wind speed and road grade. The Kalman estimator is developed for both LQIT controls to generate the estimated states accurately, based on noisy measurement, and a reference modifier is proposed to make sure that vehicle tracking error remains positive for deceleration control to avoid accidents. The simulation results in MATLAB/Simulink indicate that the LQIT control is able to track the speed reference during acceleration. Furthermore, the LQIT control has the ability to track the braking distance reference when the vehicle decelerates, and at the same time, ensure driving safety under the disturbance of gust wind by maintaining tracking error positive. The co-simulation results show that the proposed LQIT acceleration and deceleration controls are capable of improving the tracking accuracy for both speed and distance targets by up to 96.0% and 88.9% compared to the optimal control without LQIT, respectively. In addition, it is verified that the proposed control strategies are capable of handling changing traffic scenarios and emergency vehicle cut-in situations. However, the application of the designed LQIT control along with the optimal control are limited to longitudinal driving scenarios with a small turning angle. Handling large steering angles will be the focus of future work. Since the LQIT control is designed to track the given reference, future work will be carried out to optimize the weighting selection [25] in LQIT control and utilize the developed LQIT controls with the existing optimal control strategies, in real-world applications, with more uncertainties.

Author Contributions: Conceptualization, L.H. and G.Z.; methodology, L.H.; software, L.H.; validation, L.H.; writing—original draft preparation, L.H.; writing—review and editing, G.Z.; supervision, G.Z. All authors have read and agreed to the published version of the manuscript.

Funding: This research received no external funding.

Data Availability Statement: The original contributions presented in this study are included in the article. Further inquiries can be directed to the corresponding authors.

Conflicts of Interest: The authors declare no conflicts of interest.

References

1. Hawkins, T.R.; Gausen, O.M.; Strømman, A.H. Environmental impacts of hybrid and electric vehicles—A review. *Int. J. Life Cycle Assess.* **2012**, *17*, 997–1014. [CrossRef]
2. Miao, C.; Liu, H.; Zhu, G.G.; Chen, H. Connectivity-based optimization of vehicle route and speed for improved fuel economy. *Transp. Res. Part Emerg. Technol.* **2018**, *91*, 353–368. [CrossRef]

3. Li, X.; Sun, Z.; He, Z.; Zhu, Q.; Liu, D. A practical trajectory planning framework for autonomous ground vehicles driving in urban environments. In Proceedings of the 2015 IEEE Intelligent Vehicles Symposium (IV), Seoul, Republic of Korea, 28 June–1 July 2015; pp. 1160–1166.
4. Barth, M.; Boriboonsomsin, K. Energy and emissions impacts of a freeway-based dynamic eco-driving system. *Transp. Res. Part Transp. Environ.* **2009**, *14*, 400–410. [CrossRef]
5. Chen, T.; Cai, Y.; Chen, L.; Xu, X. Trajectory and velocity planning method of emergency rescue vehicle based on segmented three-dimensional quartic bezier curve. *IEEE Trans. Intell. Transp. Syst.* **2022**, *24*, 3461–3475. [CrossRef]
6. Hunt, K.; Kalkkuhl, J.; Fritz, H.; Johansen, T.; Gottsche, T. Experimental comparison of nonlinear control strategies for vehicle speed control. In Proceedings of the 1998 IEEE International Conference on Control Applications (Cat. No. 98CH36104), Trieste, Italy, 1–4 September 1998; Volume 2, pp. 1006–1010.
7. Yadav, A.K.; Gaur, P.; Jha, S.K.; Gupta, J.; Mittal, A. Optimal speed control of hybrid electric vehicles. *J. Power Electron.* **2011**, *11*, 393–400. [CrossRef]
8. Shladover, S.E.; Desoer, C.A.; Hedrick, J.K.; Tomizuka, M.; Walrand, J.; Zhang, W.B.; McMahon, D.H.; Peng, H.; Sheikholeslam, S.; McKeown, N. Automated vehicle control developments in the PATH program. *IEEE Trans. Veh. Technol.* **1991**, *40*, 114–130. [CrossRef]
9. Liu, Y.; Zhu, X.; Zhang, H.; Basin, M. Improved robust speed tracking controller design for an integrated motor-transmission powertrain system over controller area network. *IEEE/ASME Trans. Mechatron.* **2018**, *23*, 1404–1414. [CrossRef]
10. Zhu, M.; Chen, H.; Xiong, G. A model predictive speed tracking control approach for autonomous ground vehicles. *Mech. Syst. Signal Process.* **2017**, *87*, 138–152. [CrossRef]
11. Peicheng, S.; Li, L.; Ni, X.; Yang, A. Intelligent vehicle path tracking control based on improved MPC and hybrid PID. *IEEE Access* **2022**, *10*, 94133–94144. [CrossRef]
12. Liu, H.; Yan, S.; Shen, Y.; Li, C.; Zhang, Y.; Hussain, F. Model predictive control system based on direct yaw moment control for 4WID self-steering agriculture vehicle. *Int. J. Agric. Biol. Eng.* **2021**, *14*, 175–181. [CrossRef]
13. Chen, T.; Xu, X.; Cai, Y.; Chen, L.; Li, K. QPSOMPC-based chassis coordination control of 6WIDAGV for vehicle stability and trajectory tracking. *J. Frankl. Inst.* **2025**, *362*, 107458. [CrossRef]
14. Xu, S.; Peng, H.; Song, Z.; Chen, K.; Tang, Y. Design and test of speed tracking control for the self-driving lincoln MKZ platform. *IEEE Trans. Intell. Veh.* **2019**, *5*, 324–334. [CrossRef]
15. Puccetti, L.; Yasser, A.; Rathgeber, C.; Becker, A.; Hohmann, S. Speed tracking control using model-based reinforcement learning in a real vehicle. In Proceedings of the 2021 IEEE Intelligent Vehicles Symposium (IV), Nagoya, Japan, 11–17 July 2021; pp. 1213–1219.
16. Hua, L.; Dourra, H.; Zhu, G.G. Route and speed co-optimization for improving energy consumption of connected vehicles. *IEEE/ASME Trans. Mechatron.* **2024**, *29*, 2830–2838. [CrossRef]
17. Ye, Q.; Gao, C.; Zhang, Y.; Sun, Z.; Wang, R.; Chen, L. Intelligent vehicle path tracking control method based on curvature optimisation. *Sensors* **2023**, *23*, 4719. [CrossRef]
18. Hua, L.; Wei, W.; Dourra, H.; Zhu, G.G. Minimal Energy Transient Motion Control of Electrical Connected Vehicles. *IEEE/ASME Trans. Mechatron.* **2022**, *27*, 2116–2124. [CrossRef]
19. Wong, J.Y. *Theory of Ground Vehicles*; John Wiley & Sons: Hoboken, NJ, USA, 2022; pp. 8–18.
20. Antsaklis, P.J.; Michel, A.N. *Linear Systems*; Springer: Berlin/Heidelberg, Germany, 1997; Volume 8, pp. 376–378.
21. Li, J.; Wu, Z.; Li, M.; Shang, Z. Dynamic Measurement Method for Steering Wheel Angle of Autonomous Agricultural Vehicles. *Agriculture* **2024**, *14*, 1602. [CrossRef]
22. Faragher, R. Understanding the basis of the kalman filter via a simple and intuitive derivation [lecture notes]. *IEEE Signal Process. Mag.* **2012**, *29*, 128–132. [CrossRef]
23. Lopez, P.A.; Behrisch, M.; Bieker-Walz, L.; Erdmann, J.; Flötteröd, Y.P.; Hilbrich, R.; Lücken, L.; Rummel, J.; Wagner, P.; Wießner, E. Microscopic traffic simulation using sumo. In Proceedings of the 2018 IEEE 21st International Conference on Intelligent Transportation Systems (ITSC), Maui, HI, USA, 4–7 November 2018; pp. 2575–2582.
24. NASA. NASA Shuttle Radar Topography Mission (SRTM). Shuttle Radar Topography Mission (SRTM) Global. Distributed by OpenTopography. 2013. Available online: https://portal.opentopography.org/datasetMetadata?otCollectionID=OT.042013.4326.1 (accessed on 10 September 2023).
25. Zhu, G.; Rotea, M.; Skelton, R. A convergent algorithm for the output covariance constraint control problem. *SIAM J. Control Optim.* **1997**, *35*, 341–361. [CrossRef]

Disclaimer/Publisher's Note: The statements, opinions and data contained in all publications are solely those of the individual author(s) and contributor(s) and not of MDPI and/or the editor(s). MDPI and/or the editor(s) disclaim responsibility for any injury to people or property resulting from any ideas, methods, instructions or products referred to in the content.